



Optical properties of nanocrystalline magnesium aluminate spinel synthesized from industrial wastes



Emad M.M. Ewais^{a,*}, Dina H.A. Besisa^a, Ahmed A.M. El-Amir^a, Said M. El-Sheikh^b, Diaan E. Rayan^c

^a Refractory & Ceramic Materials Division (RCMD), Central Metallurgical R&D Institute (CMRDI), P. O. Box 87 Helwan, 11421 Cairo, Egypt

^b Nano-structured Materials Division, Central Metallurgical R&D Institute (CMRDI), P. O. Box 87 Helwan, 11421 Cairo, Egypt

^c Electronic Materials Division, Central Metallurgical R&D Institute (CMRDI), P. O. Box 87 Helwan, 11421 Cairo, Egypt

ARTICLE INFO

Article history:

Received 19 April 2015

Accepted 14 July 2015

Available online 16 July 2015

Keywords:

Magnesium aluminate spinel nanoparticles

Scrap

Co-precipitation method

Phase composition

Optical properties

ABSTRACT

In this work, magnesium aluminate spinel (MA) nanoparticles were synthesized via co-precipitation method using industrial wastes of magnesium and aluminum. The obtained powders were calcined at a temperature range of 650–1500 °C. The calcined powders were characterized by XRD, FT-IR, DTA, FE-SEM and HR-TEM. XRD data illustrated that the spinel MA with a crystallite size of ~3.8 nm was formed at 650 °C. Optical properties of the MA spinel revealed that the optical reflectance is highly dependent on calcination temperature. Photoluminescence analysis revealed intrinsic emission bands with high intensity centered at 390, 370 and 485 nm, when the samples are excited by a 350 nm light from a Xe lamp at room temperature. Results suggest that co-precipitation method of aluminum and magnesium wastes at low temperatures is a promising way for the production of highly pure and active nanocrystalline MA spinel with expected unique properties.

© 2015 Elsevier B.V. All rights reserved.

1. Introduction

Magnesium aluminate spinel (MgAl_2O_4) denoted as MA is one of the most outstanding optically transparent ceramics that exhibits a unique combination of optical and mechanical properties at the ambient and the elevated temperatures [1]. After being shown to be transparent in early 1960's, spinel has received considerable attention and has been the subject of numerous studies [2–8]. It has been considered to be well suited especially for armor applications because of its ideal combination of optical transparency, hardness, impact resistance, strength, modulus, ease of fabrication and crystal size capability [9–11]. In various studies, it has been shown to be superior to other available armor materials such as sapphire, AlON, soda-lime silicate glass and MgF_2 in terms of its excellent balance of performance and affordability [10,11]. Besides being an attractive transparent armor, it is also expected to serve as a high temperature and visible/infrared (IR) window material [4,12] because of its high thermo-mechanical properties with chemical inertness to strong acids and alkali solutions [5] as well as its

effective dual optical transparency in the visible and mid-IR wavelength ranges, respectively.

In addition, it possesses a unique combination of desirable properties such as high melting point, high strength at elevated temperature, high chemical inertness, low thermal expansion coefficient and high thermal shock resistance to make it an excellent refractory lining for rotary cement kilns, steel ladles, glass tank furnaces and other ceramic applications [13–17]. Moreover, MA spinel exhibits first deformation under 0.2 MPa at 2000 °C. It does not react with silica until 1737 °C, CaO or MgO until 2000 °C, α - Al_2O_3 until 1927 °C, and can be used for all metals except alkaline earth [18]. Due to its eco-friendly nature, unlike magnesia-chrome based refractories [19], the later ones are constantly being replaced by MgAl_2O_4 spinels [20].

Thus, it is important to obtain the spinel of high purity, using a simple and low cost preparation method. The preparation of magnesium aluminate powders with high purity, chemical homogeneity, control of stoichiometry, fine particle size, narrow particle size distribution, and minimum particle agglomeration with high sinter activity has received considerable attention in order to improve the material properties [21]. Numerous wet chemical methods have been employed to synthesize magnesium aluminate fine particles, including sol–gel [22,23], co-precipitation [24–26],

* Corresponding author.

E-mail address: dr_ewais@hotmail.com (E.M.M. Ewais).

hydrothermal [27,28], microwave-assisted combustion processing [29], microemulsion [30], metal-organic processing [31–34], spray drying [35], freeze drying [36], and mechanochemical synthesis [37,38] techniques. The chemical co-precipitation method [39–42] ensures proper distribution of various metal ions resulting into stoichiometric and smaller particle sized product compared to some of the others. Moreover, the process is a low cost technique suitable for the mass production compared to the other mentioned methods.

At present, most techniques used to produce MA spinel, whether they are solid state reactions or chemical synthesis, are conducted at high temperature (>800 °C). However, it is known that high temperature processing is detrimental to microstructure and in turn the properties due to the non-uniform grain growth. Therefore, low temperature synthesis of nanocrystalline powders of MA spinel should be investigated.

On the other hand, industrial wastes released from different manufacturing processes and treatment materials are produced in large quantities and have harmful effects on the environment. According to research conducted by the US Environmental Protection Agency, recycling scrap metal wastes can be quite beneficial to the environment. For example, using recycled scrap metal in place of virgin iron ore can yield 75% savings in energy, 90% savings in raw materials used, 86% reduction in air pollution, 40% reduction in water use, 76% reduction in water pollution and 97% reduction in mining wastes [43].

In 1990 total aluminum production was around 28 million tonnes (with over 8 million tonnes recycled from scrap) and today the total is close to 56 million tonnes (with close to 18 million tonnes recycled from scrap). By 2020 metal demand is projected to have increased to around 97 million tonnes (~31 million tonnes recycled from scrap).

During manufacturing of magnesium products, large amount of wastes in the form of chips and discards is produced in the machining process of castings and sheets. Approx. 1/3 of magnesium used to fabricate structural products ends as scrap, so it is really inevitable to find ways for its efficient recycling in order to keep the use of Mg and thus price at a reasonable level.

Nowadays, industrial waste materials are getting a wide exposure to the future generation of the material science world. The novelty and the idea of this work is how to convert unwanted waste materials into something useful or value-added products via an environmental friendly method for advanced applications. In this study, our group reported for the first time, the synthesis of MgAl₂O₄ spinel nanoparticles from industrial wastes of aluminum and magnesium scraps released from foundries by co-precipitation method at low temperature. Magnesium aluminate spinel was produced at different temperatures 650–1500 °C. The phase composition, thermal analysis, and microstructure of these compositions were detected using X-ray diffraction (XRD), differential thermal analysis (DTA), infrared spectrum (IR), scanning electron microscope (FE-SEM) as well as transmission electron microscope (TEM). The optical properties of the produced MA were also studied by UV-VIS-NIR spectrophotometer and photoluminescence analysis.

2. Materials and experimental procedure

2.1. Materials and processing

Aluminum and magnesium scrap released from foundries (supplied by Central Metallurgical Research & Development Institute [CMRDI], Helwan, Egypt) were used as starting materials. Ammonia solution [NH₄OH] was used during the co-precipitation to maintain the pH at 10. The chemical composition of aluminum scrap is illustrated in Table 1.

Table 1
Chemical composition of Al scraps.

Elements	Al	Zn	Mg	Cu
Percentage, %	92	3.96	2.35	1.7

An aqueous solution of magnesium nitrate was achieved by dissolving the magnesium scrap in nitric acid. The aqueous solution of aluminum nitrate was achieved by dissolving the aluminum scrap in aqua regia of 20% HCl and 20% HNO₃ acids. The stock solution used for spinel synthesis was made by dissolving magnesium and aluminum nitrates in distilled water with stirring.

In a typical synthesis process, the aqueous solution of the aluminum nitrate was added to a stirring aqueous solution of magnesium nitrate to give MgO/Al₂O₃ molar ratios of 1:1 powder. The aqueous suspended solutions were formed by the addition of NH₄OH drop by drop with constant stirring 500 rpm for 15 min to achieve good homogeneity. pH of the solution was maintained at 10 during the precipitation process. The co-precipitates were filtered off, washed with water and dried in an oven at 110 °C overnight. In order to produce MA spinel, the dry precursor was calcined in a muffle furnace up to different temperatures (650, 750, 850, 950, 1300, 1400 and 1500 °C) with a rate of heating of 10 °C/min for 2 h.

2.2. Characterization

XRD patterns of the resulting products were characterized by a Bruker D8-advance X-ray powder diffractometer with Cu K α radiation ($k = 1.5406 \text{ \AA}$). The crystallite sizes of the produced magnesium aluminate spinels were calculated from the most intense peak (311) using the Debye–Scherrer formula:

$$dRX = K\lambda/\beta \cos\theta$$

where dRX is the crystallite size, $k = 0.9$ is a correction factor to account for particle shapes, β is the full width at half maximum (FWHM) of the most intense diffraction peak (311) plane of MA spinel phase, λ is the wavelength of Cu target = 1.5406 Å, and θ is the Bragg angle.

Fourier transform infrared spectra (FTIR) spectroscopy (Model, Jasco-6300 type A, Japan spectrometer) was used at room temperature in the range of 400–4000 cm⁻¹ with a resolution of 4 cm⁻¹ to identify functional groups.

Powder morphology and microstructure of the produced magnesium aluminate spinel were examined by using backscattered electron (BSE) in the field emission scanning electron microscopy

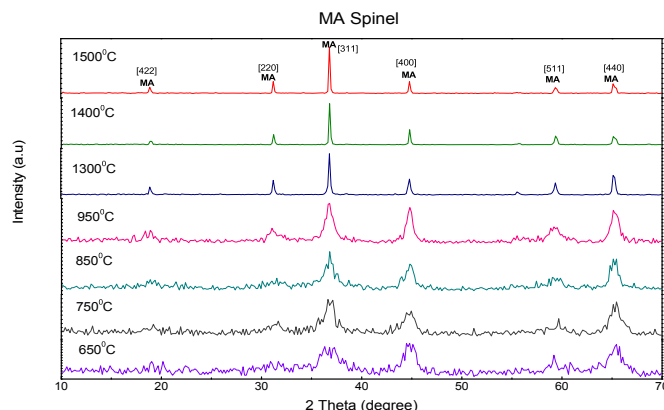


Fig. 1. XRD patterns of MA spinel powders annealed at different temperatures.

(FESEM; QUANTA FEG 250, Holland) and high resolution transmission electron microscope (HR TEM; JEM- 2100, Japan). TEM samples were prepared by dispersing the powders in acetone. Ultrasonic oscillation for 1 h was introduced to decrease the aggregation followed by placing a drop of the suspension on holey carbon film supported on copper grids.

Differential thermal analysis/thermogravimetry analysis (DTA-TG) of the precursors were performed using a DTA-TG analyzer (Model, NETZSCH STA 409C/CD, Germany) in flowing air (50 ml/min) up to 1400 °C at a heating rate of 10 K/min.

The UV–Vis absorption and diffuse reflectance spectrum were recorded at room temperature using UV-VIS-NIR spectrophotometer (Jasco-V-570 spectrophotometer, Japan) fitted with integrating sphere reflectance unit (ISN) in the wavelength range 200–2000 nm. PL spectra were recorded at room temperature using a Shimadzu RF-5301PC fluorescence spectrophotometer (Shimadzu, Kyoto, Japan) with a 50 W xenon lamp.

3. Results and discussion

XRD diffraction patterns for the produced magnesium aluminate spinel powders synthesized by co-precipitation using aluminum and magnesium scraps at different calcination temperatures for 2 h are shown in Fig. 1. It was found that magnesium aluminate spinel peaks (MgAl_2O_4 ; JCPDS card no 86–2258) with very fine crystallite size (3.8 nm) were revealed at low calcination temperature (650 °C). This means that the dried gel transformed to ultrafine powders of MgAl_2O_4 spinel phase at this temperature. The strongest three peaks of the produced powders appeared at 2θ values of 65.22°, 44.75° and 36.77°. These peaks correspond to (440), (400) and (311) diffraction planes of the MA phase, which described based on the patterns as face-centered cubic, space group: $Fd3m$, lattice parameter (a) 8.088, z (coordination number) 8. The peaks broadening of the spinel were occurred at lower temperatures of 650, 750 and 850 °C due to the small grain size formed at these temperatures relative to the other high ones. Because of the decrease of the grain size, the number of the planes in a crystal that diffract at the same angle was decreased causing the so-called peak broadening. With increasing calcination temperature, a well formed crystalline MA spinel phase was obtained. The sharp reflections of XRD peaks at high temperatures emphasize the full crystallization of spinel. The crystallite size of MA spinel phase was increased from 3.8 to 5.7 nm, when the temperature increased from 650 to 750 °C, respectively with increasing the temperature to 1500 °C, the crystallite size increased up to 173.1 nm. This means that there is a gradual increase in crystallite size as a function of the calcinations temperatures. This relationship can be ascribed to the nucleation, the growth rates of the produced

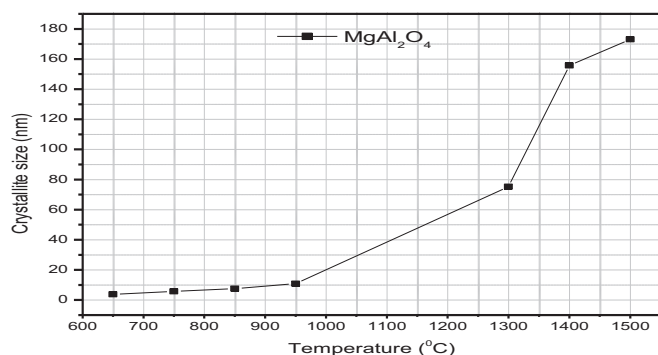


Fig. 2. Crystallite size of the MA spinel powders as a function of the calcinations temperature.

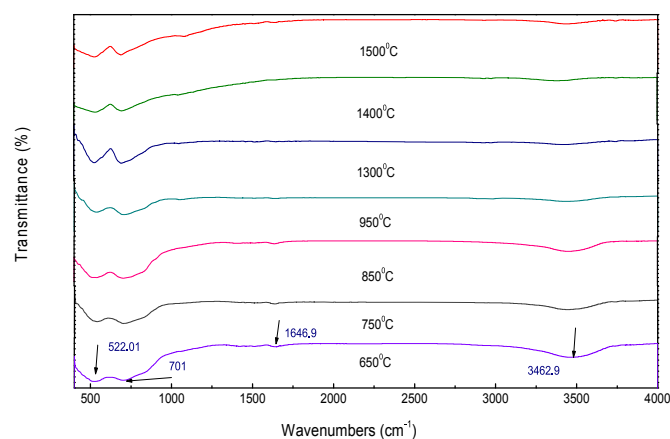


Fig. 3. FT-IR spectra of MA spinel nanopowders calcined at different temperatures.

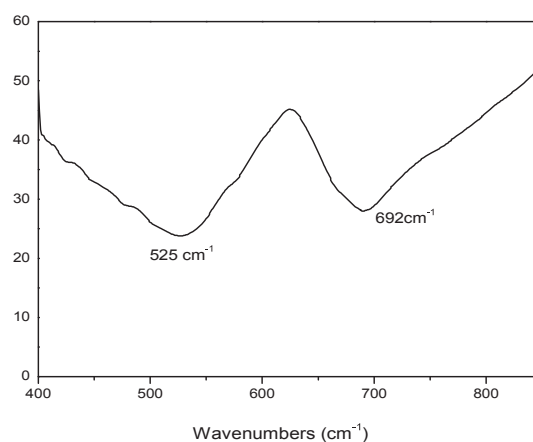


Fig. 4. Characteristic absorption band of MA spinel structure.

powders as well as the high crystallinity of the MA spinel phase with the increase of the calcination temperature. Fig. 2 illustrates the increase of the crystallite sizes of the MA spinel phase formed by increasing the calcinations temperatures. Therefore, the advantage of our work is the formation of an ultrafine nanocrystalline MA spinel phase at low temperature of 650 °C using both industrial wastes of aluminum and magnesium scraps.

The FT-IR spectra at 400–4000 cm^{-1} for the nanocrystalline MA

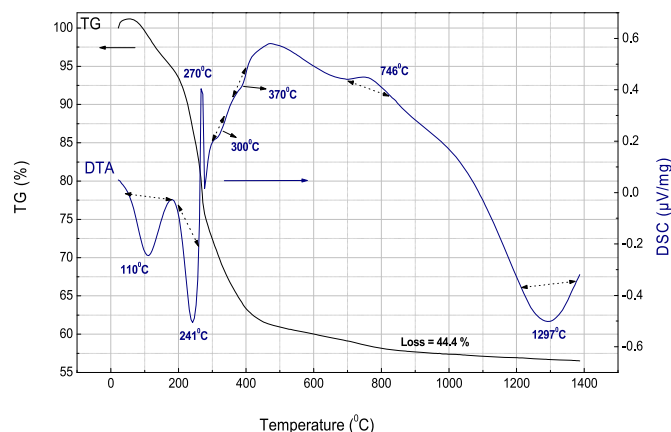


Fig. 5. DTA and TG of MA spinel nanopowders.

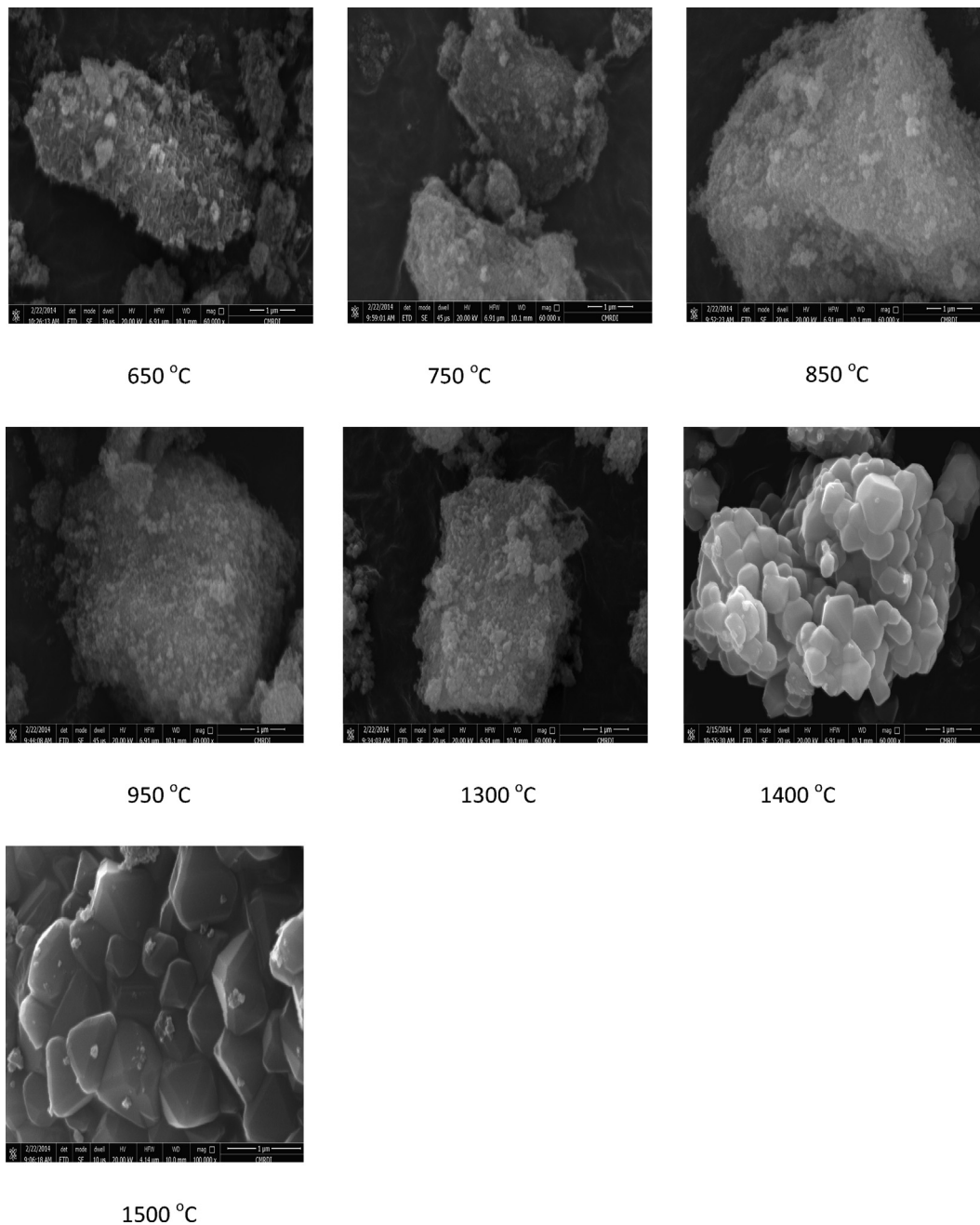


Fig. 6. FE-SEM of MA spinel calcined at different temperatures.

spinel powders calcined at different temperatures are shown in Fig. 3. This clearly shows a broad absorption band at $3150\text{--}3750\text{ cm}^{-1}$, which is the characteristic stretching vibration of hydroxylate (O–H) and the absorption band at $\approx 1643\text{ cm}^{-1}$ for H_2O vibration was obtained. No characteristic band of nitrate ions at 1464 cm^{-1} is observed from the FT-IR spectra indicating the complete decomposition of the magnesium and aluminum nitrate precursor during the heat treating processes. Significant double spectroscopic bands appeared at $522\text{--}544\text{ cm}^{-1}$ and $692\text{--}704\text{ cm}^{-1}$ are identified to be the characteristic absorption bands of MA spinel structure [44], see Fig. 4. These peaks are attributable to the vibration of AlO_6 , which built up MA spinel structure [45]. This double splitting of the high frequency band may be explained by the assumption that a certain number of Al^{3+} ions

occupy the sites in the spinel type structure. By increasing the calcinations temperature, bands of the water disappeared and the intensified absorption peaks revealed the formation of pure magnesium aluminum spinel.

In order to assess the degree of reaction occurred and the stability of the powders with respect to thermal as well as the chemical composition, MA spinel nanopowders synthesized by coprecipitation at different calcination temperatures were subjected to thermogravimetric (TG) and differential thermal analysis (DTA) (Fig. 5) up to a temperature of $1400\text{ }^\circ\text{C}$ with heating rate of 10 K/min in the air. It can be observed that in the range of $\text{RT}\text{--}200\text{ }^\circ\text{C}$, an endothermic peak at $\sim 100\text{ }^\circ\text{C}$ in DSC curve with a mass loss of $\sim 5.7\%$ appears which can be attributed to the evaporation of physisorbed moisture. The endothermic peak centered at $241\text{ }^\circ\text{C}$ with mass loss

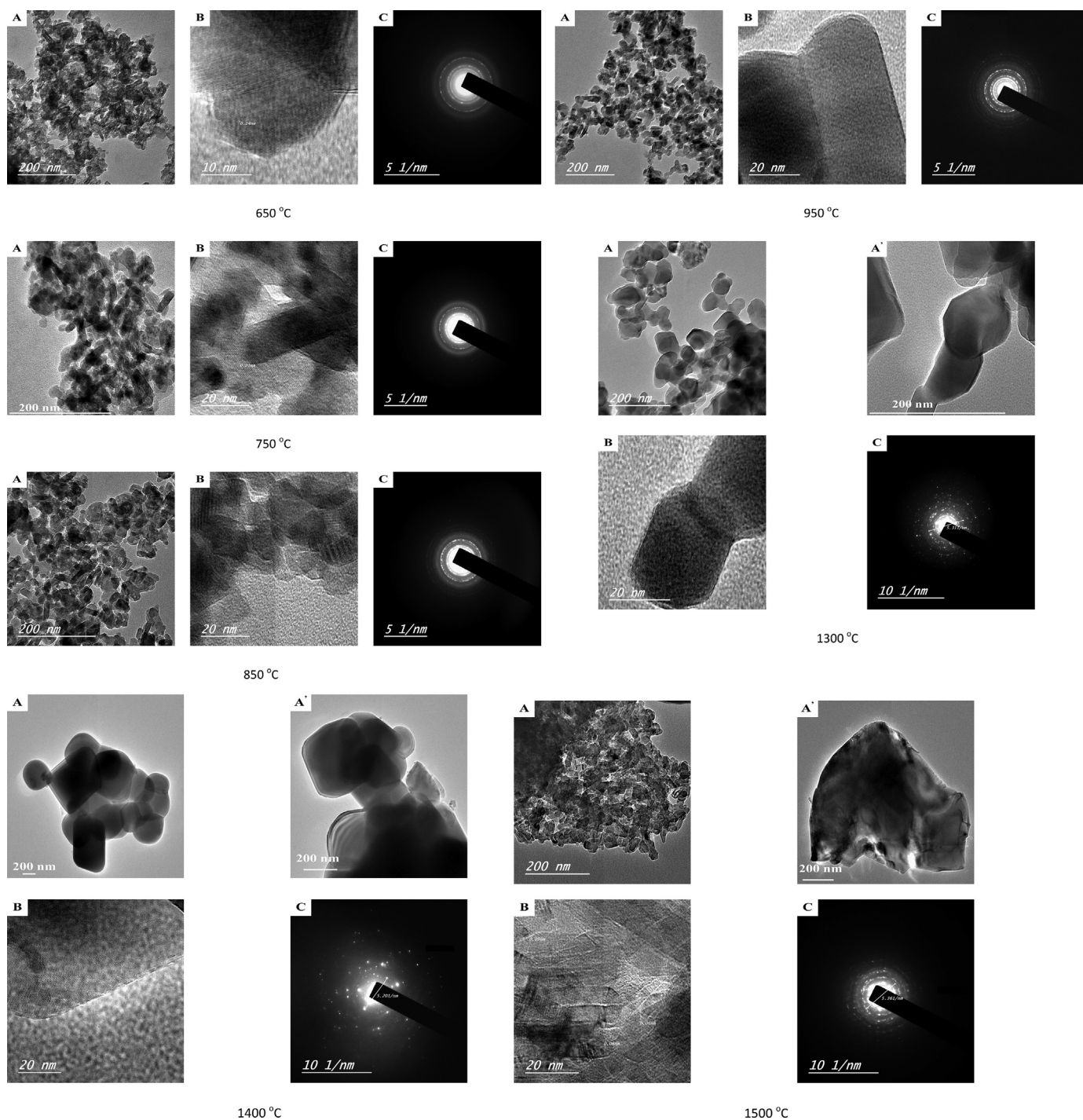


Fig. 7. TEM of calcined MA spinel at different temperatures, (A, A') TEM images, (B) HR-TEM of lattice plane, (C) SAED patterns.

of about 20% may be corresponded to the evaporation of physically bound absorbed water or/and a small amount of residual ammonia adsorbed on the surface of the sample. The outstanding and sharp exothermic peak between 260 and 300 °C centered at about 270 °C is due to the combustion and decomposition of ammonium nitrate, which takes place in the temperature range (270–300 °C). Such exothermic reaction produced ~13.6% loss of the mass. The two peaks appeared at ~300 and 370 °C correspond to the decomposition of the formed phases during the preparation procedure. This decomposition is associated with dehydroxylation of the precursors and conversion into oxides. When samples are calcined

>500 °C, these phases were decomposed and finally MA spinel crystal was produced [46]. The final weight loss (~4.5%) on the TG curve was observed in the range of 500–1300 °C which is due to the removal of residual (OH) group. The total weight loss accompanied by all stages in the TG analysis result are ~44.4%. The exothermic peak formed in the temperature range of 600–800 °C was assigned to the mass formation of MA spinel. This indicates that the solid state reaction to form magnesium aluminate spinel may occur above 600 °C. Herin we chose temperature of 650 °C as starting calcinations temperature of MA spinel structure. The relatively broad band of the peak centered at about 1300 °C in the

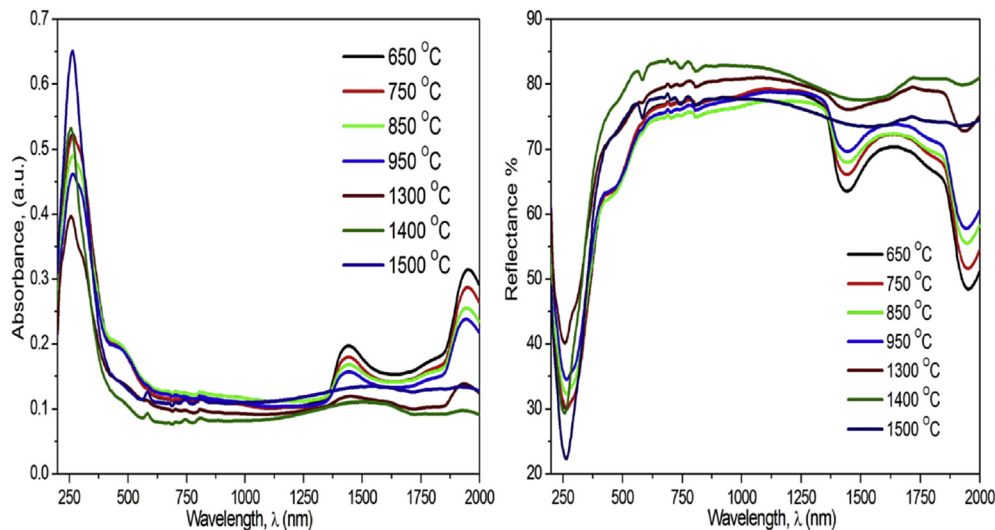


Fig. 8. Optical absorbance and reflectance spectra of samples with various different temperatures.

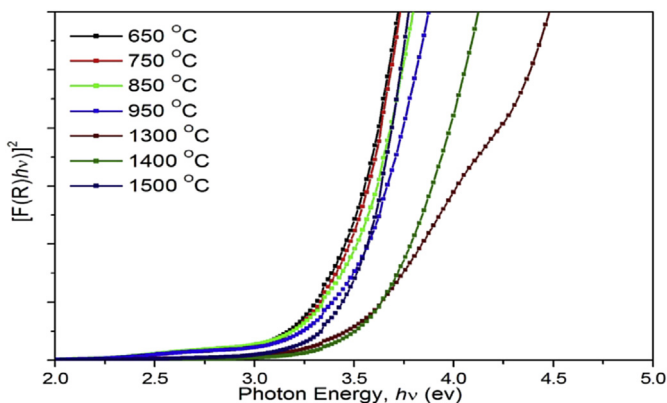


Fig. 9. Optical band gap of samples with various different temperatures.

temperature range of 1200–1400 °C may be contributed to the crystal growth of MA spinel structure [47].

Fig. 6. Shows FE-SEM images of the MA spinel powder calcined at different temperatures for 2 h. A large number of nano-MA spinel aggregates can be observed. The particle size of these aggregates was increased with increasing temperatures. MA spinel particles show a prismatic crystal structure resulting from sintering at high temperatures (>1300 °C) and grain growth during which the spinel becomes fully crystalline. It is deduced that the grain size of the MA particle increases with increasing temperature, and the crystal structure tends to be faceted.

The TEM images, SAED and lattice plane of self agglomerated MA spinel nanoparticles calcined at different temperature are shown in Fig. 7. In general, the morphology shows a bunch of very fine nanocrystals self-organized to form a bigger cluster. This degree of stacking and aggregation is owing to the high crystalline nature of obtained MA spinel and its processing without using any surfactant. It is also observed that calcinations temperature has a significant impact on the size and shape of the grains. At lower calcinations temperature (650–950 °C), morphology of MA is nanorods with a diameter of 4–7 nm and length range of 30–49 nm. In addition, there are few spherical particles with nearly about 10–30 nm in diameter. With increasing the calcinations temperature up to 950 °C, the diameter of the nanorods started to increase to 16 nm and the length started to decrease to 20 nm and

small numbers of cubic grains started to appear. At higher calcinations temperature (1300–1500 °C), the large cubic structure morphology becomes the dominant and the particle size increased to 0.2 μm length and 0.3 μm width. At high calcinations temperature, different small grains were sintered and attached to each other to form one large grain. The crystallinity of the samples is highly improved by increasing the temperature as shown in the SAED images. The selected area diffraction pattern of MA spinel calcined at low temperatures gave polycrystalline pattern. However, with increasing temperature, the pattern gave single crystal pattern. In addition, the visibility of clear lattice planes at each temperature that observed by using HR-TEM indicates the high crystalline nature of the samples. Due to the stacking and agglomeration of crystal lattice, plane image of the samples gave an image similar to the fingerprint pattern as observed in the sample calcined at 1500 °C at Fig. 7. The spacings of 2D lattice fringe (2.02, 1.42, 2.8 and 1.5 Å) of the calcined powder at different temperatures correspond to the indices of the cubic MA planes [(400), (440), (220) and (511)] with Fd3m symmetry. These results are totally agreeing with the x ray diffraction patterns of MA spinel.

The optical properties of the produced powders were examined using UV–Vis–NIR spectrophotometer using integrating sphere unit and the results are indicated in Fig. 8 and Fig. 9. Clearly, the optical reflectance (R) of the powders is highly dependent on the calcination temperature. The powders calcined at 650 °C exhibit the lowest optical reflectivity of (~60%) in the visible region. Further increases in calcination temperature resulted in highly reflective powders with an average reflectivity of ~85% in the visible region.

Also, the results revealed that the recorded absorbance is a characteristic peak of Al³⁺ and Mg²⁺ ions. The absorption peak recorded at 210 nm corresponds to the presence of Al₂O₃ nanoparticles and also the spectra of Al₂O₃ with substitution grade material [48–50]. Moreover, the defect responsible for the 260 nm absorption band may be related to Al vacancies [51–53]. Furthermore, the absorption spectra of Mg²⁺ ion consist of four bands with maxima at ~250, 355, 573 and 975 nm [54–58]. Anion vacancies define in two charge states: F⁺ and F centers are identical to oxygen vacancies with one and two electrons, respectively. Anion vacancies F⁺ centers have an absorption band at 252 nm and F centers at 247.5 nm. Neutral anion F²⁺ centers have absorption bands at 355 and 975 nm and an unidentified aggregate defect absorbs at 573 nm. The absorption spectrum of the Mg²⁺, containing

Table 2
Crystallite size (t), Lattice constant (a) and Lattice volume (V) of produced samples nanoparticles.

Name	Phases	Phase 1			Energy Gap, Eg (eV)
		Cryst. size, t (nm)	Lattice constant, a (Å)	Lattice volume, V (Å ³)	
MA 650	MgAl ₂ O ₄	3.8	8.100	531.479	3.37
MA 750	MgAl ₂ O ₄	5.7	8.093	530.103	3.39
MA 850	MgAl ₂ O ₄	7.6	8.092	529.836	3.40
MA 950	MgAl ₂ O ₄	10.8	8.096	530.572	3.46
MA 1300	MgAl ₂ O ₄	75.3	8.094	530.200	3.48
MA 1400	MgAl ₂ O ₄	155.7	8.089	529.334	3.65
MA 1500	MgAl ₂ O ₄	173.1	8.092	529.855	3.31

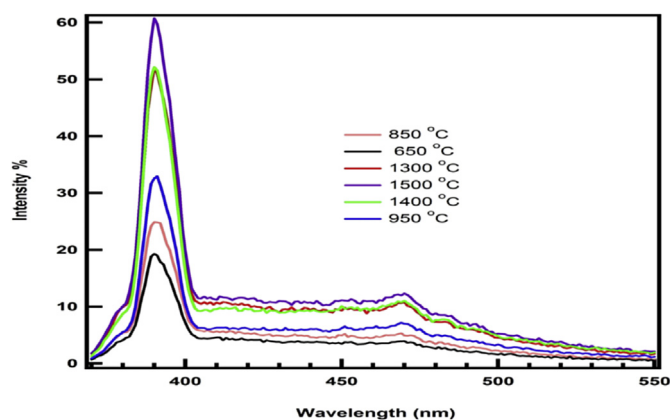


Fig. 10. PL spectra of magnesium aluminates powder produced at different temperatures.

impurities of transition elements such as chromium, iron, manganese, contains bands caused by d–d transition of these ions [59,60].

The band gap energy of the prepared MA spinel nanoparticles was estimated by extrapolating the linear portion of $(\alpha hv)^2$ versus photon energy (hv) plots using the following relation [49,50].

$$\alpha hv = A (hv - E_g)^n$$

where $\alpha = 2.303 \times \ln(I_0/I)/t$, here $\ln(I_0/I) = (100-R)/(2R)$ is the absorbance and t is the thickness of the sample. A is a constant for direct transition, hv is the photon energy, E_g is the band gap energy, $n = 1/2$ or $3/2$ for indirect allowed and indirect forbidden transitions, and $n = 2$ or 3 for direct allowed and direct forbidden transitions. Based on this relation, the extracted band gap energy of the MA spinel nanoparticles was plotted as a function of temperature, see Fig. 9.

It can be seen that with increasing the calcination temperature of MA spinel from 650 to 1400 °C, the crystallite size was increased from 3.8 to 155.7 nm and the optical band gap energy values were slightly and gradually increased from 3.37 to 3.65 eV. However, with increasing the temperature to 1500 °C, the optical band gap was suddenly decreased to 3.31 eV as seen in Table 2. From these values, it can be concluded that the energy band gap value depends on the calcinations temperature of the prepared MA spinel and hence the crystallite size. The higher temperature and largest crystallite size result in the large band gap value and vice versa. These results are in agreement with the reported data [61].

In general, the optical phenomenon of spinel MA spinel can be attributed to its special cubic crystal structure system. In perfect normal MgAl₂O₄ spinel, the Mg²⁺ ions occupy tetrahedral 8a sites and Al³⁺ ions occupy octahedral 16d sites. In reality, there is a degree of disorder between the two cations sites. So that, some tetrahedral sites are occupied by Al³⁺ ions and some octahedral

sites are occupied by Mg²⁺ ions. This departure from the normal spinel structure causes pairs of antisite defects and in turn a degree of inversion (inverse spinel crystal structure). Most synthetic MA crystals have an inversion parameter of ≈ 0.2 [62,63]. This anti-site defects plays an important role in ion-surface interaction process and thus on the electrical and optical behaviors of MA spinel powders [62]. Moreover, different computational models have been investigated to study the order-disorder behavior of MA spinel. They found that, cations disordering of Mg and Al between the octahedral and tetrahedral sites is basically depends on the calcinations temperature [64]. With increasing temperature >1400 °C, a rapid exchange between the tetrahedral and octahedral sites occurs and causing disorder state of MA spinel structure which explains: why the optical band gap energy of MA decreased with further increase of the calcined temperature above 1400 °C.

Fig. 10 shows the PL spectra of magnesium aluminates powder produced at different temperatures 650–1500 °C. PL intrinsic emission bands with high intensity centered at 390, 370 and 485 nm were recorded when the samples are excited by a 350 nm light from a Xe lamp at room temperature. The position of these emission lines is consistent with that reported earlier for metal aluminates [1–5]. PL data show strong emission bands in UV (390 nm) region and blue emission bands with weak intensity in the blue region at 470 and 485 nm. A broad and strong peak in UV region and a weak bands in the blue region confirmed the good crystallinity of the prepared MA nanoparticles. The PL intensity is controlled by the number of charge transfers between Al³⁺ at octahedral sites and its surrounding O²⁻ ions [65–69]. In addition, the emission maximum in this work suggests surface defects, such as oxygen vacancies. These defects provide donor levels near the conduction band edge of the oxide. Moreover, the emission peaks obviously shift to the region of long wavelength with an increase in calcination temperatures, which is in good agreement with the results obtained by XRD data. This shift may be due to the particle-forming effect and the increase of the size of the nanoparticles. The blue shift in the emission peaks might be caused by the quantum size effect in MA nanostructures.

This observation rather confirms that this sample almost consists of magnesium aluminates [65–70]. The differences between these recorded values were attributed to the difference in calcination temperatures.

4. Conclusions

Single nanocrystalline MgAl₂O₄ spinel powders were successfully synthesized by co-precipitation method using industrial wastes of Al and Mg scraps. Our approach helps to overcome the high cost and complex nature of the existing processes. In addition, it gave a useful, inexpensive and environmentally-friendly way to convert waste materials into advanced material. Ultrafine spinel powders (<50 nm) were obtained at different calcinations temperatures. The effect of temperature on particles morphology and

crystallinity was investigated. MA spinel nanorods were formed at low temperatures without using any additives or aiding agents. Due to the reactivity of such structure, it can be expected to be used in several high technological applications such as nanoelectronics and nano-optoelectronic systems. The results also revealed that increasing calcinations temperatures increased the crystallinity and particle size of spinel due to the thermal sintering of MA spinel. Investigations of the optical properties showed that, they are mainly depending on calcinations temperatures and crystallite size of the obtained MA spinel samples. The results suggest that co-precipitation method of aluminum and magnesium scraps at low temperatures is a promising way for the production of highly pure and active magnesium aluminate spinel nanocrystalline materials with expected unique optical properties.

References

- [1] Arcan F. Dericioglu, Aldo R. Boccaccini, Ivo Dlouhy, Yutaka Kagawa, J. Mater. Trans. 46 (5) (2005) 996–1003.
- [2] R.J. Bratton, J. Am. Ceram. Soc. 57 (1974) 283–286.
- [3] M.C.L. Patterson, J.E. Caiazza, D.W. Roy, Proc. SPIE 4102 (2000) 59–68.
- [4] D.W. Roy, J.L. Hastert, Ceram. Eng. Sci. Proc. 4 (1983) 502–509.
- [5] K.E. Green, J.L. Hastert, D.W. Roy, Proc. SPIE 1112 (1989) 2–8.
- [6] D.W. Roy, Proc. SPIE 297 (1981) 13–18.
- [7] K. Hamano, S. Kanzaki, Yogyo-Kyokai-Shi 85 (1977) 225–230.
- [8] S. Kanzaki, K. Saito, Z. Nakagawa, K. Hamano, Yogyo-Kyokai-Shi 86 (1978) 485–491.
- [9] G. Gilde, P. Patel, M. Patterson, Proc. SPIE 3705 (1999) 94–104.
- [10] D.W. Roy, G.G. Martin, J. Proc. SPIE 1760 (1992) 2–13.
- [11] J.J. Swab, J.C. LaSalvia, G.A. Gilde, P.J. Patel, M.J. Motyka, Ceram. Eng. Sci. Proc. 20 (1999) 79–84.
- [12] D.S. Tsai, C.T. Wang, S.J. Yang, S.E. Hsu, Mater. Manuf. Process. 9 (1994) 709–719.
- [13] K.H. Hwang, K.D. Oh, R.C. Bradt, in: Proc. UNITER'97, 1997, pp. 1575–1580.
- [14] M.A. Sainz, A. Mazzoni, E. Aglietti, A. Caballero, in: Proc. UNITER'97, 1995, pp. 387–392.
- [15] Y. Urita, K. Yamaguchi, I. Takita, K. Furuta, Y. Natsuo, Taikabutsu 45 (11) (1993) 664–672.
- [16] C. Baudin, R. Martinez, P. Pena, J. Am. Ceram. Soc. 78 (7) (1995) 1857–1862.
- [17] E. Ruh, Japan and the United States, Am. Ceram. Soc. Bull. 63 (9) (1984) 1140–1142.
- [18] Belding J.H., Letzgs E.A, US Patent No. 3 950 504, 13 April, 1976.
- [19] S.E. Laurich-McIntyre, R.C. Bradt, in: Proc. Unitercer-93, Congress, Sao Paulo, Brazil, 1993, pp. 256–264.
- [20] D. Son, Y. Kim, J. Yang, in: Proc. UNITER'97, 1997, pp. 241–246.
- [21] B. Alinejad, H. Sarpoolaky, A. Beitollahi, A. Saberi, S. Afshar, Mater Res. Bull. 43 (2008) 1188.
- [22] M.J. Iqbal, S. Farooq, Mater Sci. Eng. B 136 (2007) 140.
- [23] J. Guo, H. Lou, H. Zhao, X. Wang, X. Zheng, Mater Lett. 58 (2004) 1920.
- [24] M.F. Zawrah, H. Hamaad, S. Meky, Ceram. Int. 33 (2007) 969.
- [25] A. Wajler, H. Tomaszewski, E. Drozd_z-Cieśla, H. Weglarz, Z. Kaszkur, J. Eur. Ceram. Soc. 28 (2008) 2495, <http://dx.doi.org/10.1016/j.jeurceramsoc.2008.03.013>.
- [26] X.L. Duan, C.F. Song, Y.C. Wu, F.P. Yu, X.F. Cheng, D.R. Yuan, J. Non-Cryst. Solids 354 (2008) 3516.
- [27] W.J. Dawson, Ceram. Bull. 67 (1988) 1673.
- [28] D. Andeen, L. Loeffler, N. Padture, F.F. Lange, J. Cryst. Growth 259 (2003) 103.
- [29] I. Ganesh, R. Johnson, G.V.N. Rao, Y.R. Mahajan, S.S. Madavendra, B.M. Reddy, Ceram. Int. 31 (2005) 67.
- [30] F. Meyer, A. Dierstein, C.H. Beck, W. Härtl, R. Hempelmann, S. Mathur, M. Veith, Nano Struct. Mater 12 (1999) 71.
- [31] A. Saberi, F.G. Fard, H. Sarpoolaky, M.W. Porada, T. Gerdes, R. Simon, J. Alloys Compd. 462 (2008) 142, <http://dx.doi.org/10.1016/j.jallcom.2007.07.101>.
- [32] R. Ianoş, I. Lazău, C. Păcurariu, P. Barvinschi, Mater Res. Bull. 43 (2008) 3408.
- [33] C. Păcurariu, I. Lazău, Z. Ecsedi, R. Lazău, P. Barvinschi, G. Mărginean, J. Eur. Ceram. Soc. 27 (2007) 707.
- [34] Z. Haijun, J. Xiaolin, Y. Yongjie, L. Zhanjie, Y. Daoyuan, L. Zhenzhen, Mater Res. Bull. 39 (2004) 839.
- [35] X.L. Pan, S.S. Sheng, G.X. Xiong, K.M. Fang, S. Tudyka, N. Stroth, H. Brunner, Coll. Surf. A Physicochem Eng. Asp. 179 (2001) 163.
- [36] C.T. Wang, L.S. Lin, S.J. Yang, J. Am. Ceram. Soc. 75 (1992) 2240.
- [37] E. Yalamac, S. Akkurt, M. Gıftcioglu, Key Eng. Mater 264–268 (2003) 53.
- [38] D. Domanski, G. Urretavizcaya, F.J. Castro, F.C. Gennari, J. Am. Ceram. Soc. 87 (2004) 2020.
- [39] M.M. Rashad, M. Radwan, M.M. Hessien, J. Alloys Compd. 3 (2008) 304.
- [40] M.I. Iqbal, M.N. Ashiq, Chem. Eng. J. 136 (2008) 383.
- [41] M.I. Iqbal, M.N. Ashiq, P.H. Gomez, J.M. Munoz, J. Magn. Magn. Mater 320 (2008) 881.
- [42] M.M. Hessien, M.M. Rashad, K. El-Barawy, J. Magn. Magn. Mater 320 (2008) 336.
- [43] Benefits of Recycling Scrap Metal, Report of Norstar Steel Recycler, 2011.
- [44] J. Chandradass, Ki Hyeon Kim, J. Ceram. Proc. Res. 11 (1) (2010) 96–99.
- [45] S. Kurien, S. Sebastian, J. Mathew, K.C. George, Indian J. Pure Appl. Phys. 42 (2004) 926–933.
- [46] H. Zhang, X. Jia, Z. Liu, Z. Li, Mater. Lett. 58 (2004) 1625.
- [47] S.K. Behera, P. Barpanda, S.K. Pratihari, S. Bhattacharyya, Mater. Lett. 58 (2004) 1451.
- [48] V. Piriyaowong, V. Thongpool, P. Asanithi, P. Limsuwan, Preparation and Characterization of Alumina Nanoparticles in Deionized Water Using Laser Ablation Technique, J. Nanomater. 2012 (2012) 1–6.
- [49] H. Chang, Y.C. Chang, J. Mat. Proc. Tech. 207 (1–3) (2008) 193–199.
- [50] V.S. Kortov, S.V. Nikiforov, I.I. Milman, E.V. Moiseykin, Radiat. Meas. 38 (4–6) (2004) 451–454.
- [51] G.W. Arnold, G.B. Krefft, B. CNorris, Appl. Phys. Lett. 25 (1974) 540.
- [52] E.W.J. Mitchell, J.D. Higden, P.D. Townsend, Philos. Mag. 5 (1960) 1013.
- [53] Op Gibbs, in: W.D. Kingery (Ed.), Conference on the Kinetics of High-temperature Processes, Wiley, New York, 1959, p. 21.
- [54] V. Skvortsova, L. Trinkl, Transition metal ions luminescence in neutron irradiated magnesium oxide, 11th Europhysical Conference on Defects in Insulating Materials (EURODIM 2010), IOP Conf. Ser. Mater. Sci. Eng. 15 (2010) 012055.
- [55] B. Henderson, J.E. Wertz, Defects in Alkaline Earth Oxides with Application to Radiation Damage and Catalysis, 1977 (London).
- [56] M.A. Monge, A.I. Popov, C. Ballesteros, R. Gonzalez, Y. Chen, E.A. Kotomin, Phys. Rev. B 62 (2000) 9299.
- [57] Y. Chen, R. Williams, W.A. Sibley, Phys. Rev. 182 (1969) 960.
- [58] L.E. Halliburton, L.A. Kappers, Solid State Commun. 26 (1978) 111.
- [59] M. Okada, T. Kawakubo, T. Seiyama, M. Nakagawa, Phys. Stat. Sol. (B) 144 (1987) 903.
- [60] N. Mironova, U. Ulmanis, Radiation Defects and Iron Group Metal Ions in Oxides, 1988 (Riga, in Russian).
- [61] S. Benramache, O. Belahssen, A. Guettaf, A. Arif, J. Semicond. 35 (4) (2014) 1–4.
- [62] J.A. Ball, S.T. Murphy, R.W. Grimes, D. Bacorisen, R. Smith, B.P. Uberuaga, K.E. Sickafus, J. Solid State Sci. 10 (2008) 717–724.
- [63] Siby Kurien, Shajo Sebastian, Jose Mathew, K.C. George, Indian J. Pure Appl. Phys. 42 (2004) 926–933.
- [64] S.A.T. Redfern, R.J.H. Harrison, H.S. O'Neill, D.R.R. Wood, Am. Mineral. 84 (1999) 299–310.
- [65] R.T. Kumar, N.C.S. Selvam, C. Ragupathi, L.J. Kennedy, J.J. Vijay, Powder Technol. 224 (2012) 147–154.
- [66] C. Ragupathia, J.J. Vijayaa, L. John Kennedy, M. Bououdinac, Ceram. Int. 40 (2014) 13067–13074.
- [67] C. Ragupathi, J.J. Vijaya, P. Surendhar, L.J. Kennedy, Polyhedron 72 (2014) 1–7.
- [68] C. Ragupathi, J.J. Vijaya, L.J. Kennedy, M. Bououdina, Mater. Sci. Semicond. Process. 24 (2014) 146–156.
- [69] C. Ragupathia, J. Judith Vijayaa, L. John Kennedy, Mater. Sci. Eng. B 184 (2014) 18–25.
- [70] V.T. Gritsyna, I.V. Afanasyev-Charkin, Yu.G. Kazarinov, K.E. Sickafus, Vacuum 81 (2006) 174–178.